Resonant pull-in of a double-sided driven nanotube-based electromechanical resonator

Changhong Ke[a)]
Department of Mechanical Engineering, State University of New York at Binghamton, Binghamton, New York 13902-6000, USA

(Received 30 July 2008; accepted 1 December 2008; published online 16 January 2009)

We theoretically investigate the electromechanical dynamics of a double-sided driven cantilevered nanotube-based electromechanical resonator. Closed-form analytical solutions capable of predicting the steady-state resonant oscillation of the device and its resonant pull-in conditions are derived using an energy-based method and are verified through a comparison with numerical simulations. Our closed-form formulas clearly reveal the complex relationship among the device geometry, driving voltages, and the device's electromechanical dynamics. Our results show that the stable steady-state spanning range of the resonating cantilever can reach up to 90% of the gap between the actuation electrodes, which substantially exceeds the previously reported quasistatic pull-in limit for cantilevered nanotube-based nanoelectromechanical systems and the resonant pull-in limit for double-sided driven microelectromechanical gyroscopes. Our results also reveal that the processes of tuning the resonant frequency of the resonator and controlling its stable steady-state oscillation amplitude can be decoupled and controlled separately by controlling the dc and ac components in the driving signal. The unique behavior of the large stable steady-state resonant oscillation range, which is independent of the electrostatic-force-induced resonant frequency tuning, makes this double-sided driven resonator attractive for many applications, such as tunable sensors for detecting ultratiny mass and force and tunable electronics. The results reported in this paper are useful to the optimal design of novel nanotube- or nanowire-based double-sided driven electromechanical resonators. © *2009 American Institute of Physics*. [DOI: 10.1063/1.3065534]

I. INTRODUCTION

Nanoscale electromechanical resonators are currently pursued for a variety of applications, such as signal processing,[1,2] sensors for mechanical, electrical, or magnetic forces,[3–5] and detectors for chemical and biological agents.[6–8] Carbon nanotubes (CNTs),[9] a type of high aspect ratio one-dimensional nanostructures with extraordinary mechanical and electrical properties and chemical stability,[10–17] have been considered as ultimate building blocks for nanoelectromechanical systems (NEMSs). Below we briefly survey the CNT-based NEMS resonators reported in the literature and their unique electromechanical behaviors and applications. One of the earliest works on the electrostatic excitation of CNTs was reported by Poncharal *et al.*[18] They demonstrated that oscillating nanotube cantilevers can work as sensitive nanobalances for nanoscale particles. Sazonova *et al.*[5] proposed a fixed-fixed nanotube-based tunable oscillator. The dc component in the driving signal produces a static electrostatic force, which is used to control the tension in the nanotube beam, and thus its natural frequency. The ac component is used to excite the resonance of the beam. They demonstrated that this novel device can operate as an ultrasensitive force transducer with the force sensitivity up to 5×10^{-18} N. Peng *et al.*[19] developed a fixed-fixed nanotube-based resonator with a fundamental mode frequency over 1.3 GHz and mass detection sensitivity of 10^{-18} g. It is expected that NEMS resonators are superior to their microelectromechanical system (MEMS) predecessors in many aspects, such as size and integration level, working frequency, mass and force sensitivity, and energy consumption.

From a design point of view, CNTs serve as the movable electromechanical components in the aforementioned resonators and are configured as cantilevered or fixed-fixed beams. Because a cantilevered beam has significantly lower stiffness than a comparable fixed-fixed beam, its resonant frequency is also much lower. Similarly, cantilevers require significantly lower driving voltages to reach a certain oscillation amplitude than comparable fixed-fixed beams. Regarding the excitation scheme, electromechanical components of resonators can be electrostatically actuated in either a single- or double-sided manner. Studies on nanotube- or nanowire-based NEMS resonators reported in the literature through both modeling[20–23] and experiments[5,18,19,24–32] have focused on single-sided driven devices. NEMS resonators with a double-sided excitation scheme were little explored. It is noted that the double-sided driven scheme has been employed in the actuation of vibrational MEMS, such as gyroscopes,[33] microphones,[34] and comb drives.[35] Moreover, a double-sided actuated CNT-based memory element which operates in the quasistatic regime has recently been proposed.[36] Therefore, more efforts, including both theoretical modeling and experiments, are needed to the development of double-sided driven NEMS resonators.

In this paper, we theoretically investigate the electromechanical dynamics of a double-sided driven cantilevered

[a)]Electronic mail: cke@binghamton.edu; Tel.: 607-777-4782; FAX: 607-777-4620.

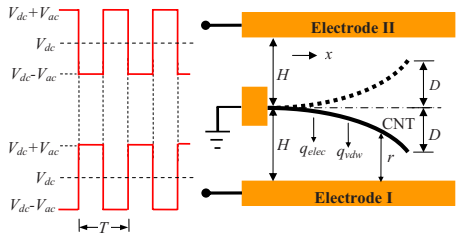

FIG. 1. (Color online) Schematics of a double-sided driven cantilevered nanotube-based electromechanical resonator (right) and driving signals (left).

nanotube-based electromechanical resonator using both a numerical method and an energy-based analytical method. Our study focuses on examining the stable steady-state (S-S) resonant oscillation and resonant pull-in (RPI) phenomenon of this device, as many applications require that the device operates in resonance for maximized oscillation amplitude. Our results also reveal the unique resonant frequency tuning capabilities of this double-sided driven resonator.

The resonator configuration employed in our study is schematically shown in Fig. 1 (right). The device comprises a conductive CNT cantilever with length L, which is actuated by two parallel-plate electrodes (I and II). Both electrodes have an equal separation with the nanotube, H. For simplicity but not to lose the generality, we employ the square-wave signals as illustrated in Fig. 1 (left) as the driving signals in our study. Both signals have the same dc bias V_{dc} and ac amplitude V_{ac}, as well as the same period T. There is a 180° difference in phase between their ac components. Forces acting on the nanotube cantilever from the parallel-plate actuator include electrostatic forces and van der Waals forces from the respective interaction between the nanotube cantilever and both electrodes. These forces are opposed by friction forces from the mechanical damping in the system. The oscillation of the cantilever induced by both driving signals is symmetric with respect to its original unactuated position, meaning zero static deflection of the cantilever beam. From a system point of view, the net added energy to the resonator shown in Fig. 1 by the van der Waals interactions in one oscillation cycle is zero due to the symmetric oscillation of the nanotube cantilever. Therefore, the added energy to the system is the electrostatic energy provided by the parallel-plate electrodes or the power supply. The dissipated energy from the system includes the energy loss due to the mechanical damping and the energy loss due to Joule heating from the electrical resistance in the wiring and the nanotube beam. For each oscillation period T, if the added energy is equal to the dissipated energy, the oscillation of the nanotube cantilever reaches its equilibrium or S-S. If the added energy cannot be balanced by the dissipated energy, dynamic pull-in,[37] or RPI when the nanotube cantilever is in resonance, takes place and the cantilever beam subsequently snaps onto one of the electrodes. The dynamic pull-in phenomenon is an unstable process and typically leads to device failure. Therefore, the stable S-S oscillation range of the resonator is limited by its RPI.

II. MODELING

A. Governing equation

The motion of the oscillating nanotube cantilever as shown in Fig. 1 is assumed to be in the small or linear deformation regime and is governed by[22]

$$\rho A\frac{\partial^2 r}{\partial t^2}+c\frac{\partial r}{\partial t}+EI\frac{\partial^4 r}{\partial x^4}=q_{\text{elec}}+q_{\text{vdW}}, \tag{1}$$

where x is the position along the nanotube, $r(x,\ t)$ is the gap between the nanotube and electrode I, E is the Young's modulus, I is the moment of inertia [for nanotubes, $I=(\pi/4)(R_{\text{ext}}^4-R_{\text{int}}^4)$, R_{ext} and R_{int} are their outer and inner radii, respectively], ρ and A are the density and cross-sectional area of the nanotube, respectively, and c is the damping factor, defined as $c=\rho A\omega_n/Q$, in which ω_n is the natural frequency of the nanotube cantilever and Q is the quality factor. q_{elec} and q_{vdW} represent the per-unit-length electrostatic and van der Waals forces acting on the nanotube cantilever, respectively. q_{elec} is given by[38,39]

$$q_{\text{elec}}=\begin{cases}\dfrac{1}{2}\dfrac{dC_p(r)}{dr}(V_{\text{dc}}+V_{\text{ac}})^2+\dfrac{1}{2}\dfrac{dC_p(2H-r)}{dr}(V_{\text{dc}}-V_{\text{ac}})^2, \\ \qquad 0\le t\le\dfrac{T}{2}, \\ \dfrac{1}{2}\dfrac{dC_p(r)}{dr}(V_{\text{dc}}-V_{\text{ac}})^2+\dfrac{1}{2}\dfrac{dC_p(2H-r)}{dr}(V_{\text{dc}}+V_{\text{ac}})^2, \\ \qquad \dfrac{T}{2}<t\le T,\end{cases} \tag{2}$$

where $C_p(r)$ is the per-unit-length capacitance between the nanotube and electrode I and is given by[40] $C_p(r)=2\pi\varepsilon_0[\cosh^{-1}(1+r/R_{\text{ext}})]^{-1}$ assuming that both electrode planes are infinite and considering only the uniform electrical charges along the side surface of the nanotube cylinder. Employing the continuum model[38] based on the Lennard-Jones potential[41] and assuming that both electrodes are N-layer graphite sheets (interlayer distance $d=0.335$ nm), the net q_{vdW} acting on the nanotube can be approximated by[22]

$$q_{\text{vdW}}=\pi\sigma^2C_6\sum_{R=R_{\text{int}}}^{R=R_{\text{ext}}}\left(R\sum_{n=1}^{N}\int_{-\pi}^{\pi}\left(\frac{1}{[(n-1)d+r+2R(1+\sin\theta)]^5}-\frac{1}{[(n-1)d+(2H-r)+2R(1+\sin\theta)]^5}\right)d\theta\right), \tag{3}$$

where $\sigma\cong 114\ \text{nm}^{-3}$ is the carbon atom density for graphite and $C_6=15.2$ eV Å^6 is a constant coefficient for carbon-carbon interactions. It is noted that Eq. (3) only considers the attractive term of the van der Waals force because the repulsive term is negligible here.

B. Analytical analysis

In this section, we derive the closed-form analytical solutions to predict the S-S resonant oscillation and the RPI conditions of the double-sided driven nanotube-based electromechanical resonator using an energy-based method.[33,42] When the nanotube cantilever oscillates at its tuned resonant

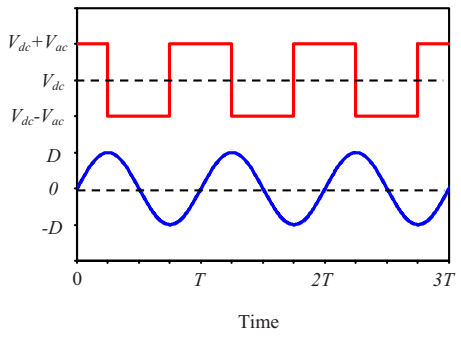

FIG. 2. (Color online) Schematics of the driving signal applied on electrode I (red curve) and the oscillation motion of the nanotube cantilever tip (blue curve).

frequency ω_{tun}, the S-S oscillation of the cantilever beam $w(x,t)$ is assumed to follow a sinusoidal function with a 90° phase lag with respect to the driving signal applied on electrode I as illustrated in Fig. 2. According to the boundary conditions at both ends of the cantilever, the shape of the deflected nanotube cantilever is assumed to follow a fourth-order polynomial, i.e., $w(x,t)=(D/3)[(x/L)^4-4(x/L)^3+6(x/L)^2]\sin(\omega_{tun}t)$, in which D is the oscillation amplitude of the nanotube cantilever tip, as shown in Fig. 1.

The energy loss due to mechanical damping in one oscillation cycle is given by

$$\Delta E_{damp}=-\int_0^L\int_0^T c\left(\frac{\partial w(x,t)}{\partial t}\right)^2 dtdx=-\frac{104\pi Lc\omega_{tun}D^2}{405}. \tag{4}$$

Noticing that the natural frequency of the cantilever beam $\omega_n=(3.516/L^2)\sqrt{EI/\rho A}$, Eq. (4) is rewritten as

$$\Delta E_{damp}=-3.175\frac{\pi EID^2}{QL^3}\frac{\omega_{tun}}{\omega_n}. \tag{5}$$

We assume that the energy loss due to Joule heating in the electrical wiring is small relative to the energy loss due to the mechanical damping. Therefore the dissipated energy from the system can be approximated by ΔE_{damp}.

The energy pumped into the system from the power supply in one oscillation cycle is calculated as the work done by the electrostatic force acting on the nanotube in one cycle, namely,

$$\Delta E_{add}=\int_0^L\int_0^T q_{elec}\frac{\partial w(x,t)}{\partial t}dtdx=8\pi\varepsilon_0 V_{dc}V_{ac}S(D), \tag{6}$$

in which

$$S(D)=\int_0^L\left\{\left[\cosh^{-1}\left(1+\frac{(H-w)}{R_{ext}}\right)\right]^{-1}-\left[\cosh^{-1}\left(1+\frac{(H+w)}{R_{ext}}\right)\right]^{-1}\right\}dx. \tag{7}$$

It is noted that $2\pi\varepsilon_0 S(D)$ represents the difference between two capacitances: one between the CNT and electrode I and the other between the CNT and electrode II. Assuming that $H-D\gg R_{ext}$, $S(D)$ can be approximated by[43]

$$S(D)\approx\int_0^L\left\{\left[\ln\left(\frac{2(H+R_{ext})}{R_{ext}}\left(1-\frac{w}{H+R_{ext}}\right)\right)\right]^{-1}-\left[\ln\left(\frac{2(H+R_{ext})}{R_{ext}}\left(1+\frac{w}{H+R_{ext}}\right)\right)\right]^{-1}\right\}dx. \tag{8}$$

The oscillation of the cantilever reaches its S-S when the added energy is equal to the dissipated energy, i.e.,

$$\Delta E_{elec}+\Delta E_{damp}=0. \tag{9}$$

Therefore, the S-S resonant oscillation of the device is given by

$$S(D)=\frac{0.397EID^2}{\varepsilon_0 V_{dc}V_{ac}QL^3}\frac{\omega_{tun}}{\omega_n}=\frac{0.549V_{SPI}^2}{QV_{dc}V_{ac}}\frac{\omega_{tun}}{\omega_n}\frac{LD^2}{\xi^2(H+R_{ext})^2}, \tag{10}$$

where

$$V_{SPI}=0.85\frac{H+R_{ext}}{L^2}\ln\left(\frac{2(H+R_{ext})}{R_{ext}}\right)\sqrt{\frac{EI}{\varepsilon_0}}$$

is the quasistatic pull-in voltage of cantilevered nanotube devices with the single-sided electrostatic actuation, which was derived and experimentally verified in our previous study,[42] and $\xi=\ln[2(H+R_{ext})/R_{ext}]$.

Using the lumped model, the tuned resonant frequency of the actuated nanotube cantilever is given by

$$\frac{\omega_{tun}}{\omega_n}=\sqrt{1+\frac{k_{elec}+k_{vdW}}{k_{elas}}}, \tag{11}$$

where k_{elas}, k_{elec}, and k_{vdW} are the spring constants corresponding to the elastic, electrostatic, and van der Waals interactions, respectively, and they can be calculated by taking the second-order derivative of the respective energy with respect to the deflection of the cantilever. For simplicity, we only consider k_{elas} and k_{elec} in the analysis of the tuned resonant frequency because they play dominant roles in the resonant frequency tuning. We rewrite the displacement of the nanotube cantilever as $w=(w_L/3)[(x/L)^4-4(x/L)^3+6(x/L)^2]$, in which w_L is the displacement of the cantilever tip. For the oscillation of the cantilever tip as shown in Fig. 2, $w_L=D\sin(\omega_{tun}t)$. The stored elastic energy from the deflection of the cantilever is

$$E_{elas}=\frac{EI}{2}\int_0^L\left(\frac{d^2w}{dx^2}\right)^2dx=\frac{8EI}{5L^3}w_L^2. \tag{12}$$

Therefore, the mechanical spring constant is obtained as

$$k_{elas}=\left.\frac{\partial^2 E_{elas}}{\partial w_L^2}\right|_{w_L=0}=\frac{16EI}{5L^3}. \tag{13}$$

Because the electrostatic energy is proportional to the square of the driving voltage, we only consider the electrostatic energy generated by the constant voltage component in both driving signals in the calculation of the electrical spring constant, which is given by

$$E_{\text{elec}} = \frac{V_{\text{dc}}^2 + V_{\text{ac}}^2}{2} \int_0^L [C_p(H - w_L) + C_p(H + w_L)]dx. \quad (14)$$

By using the approximation as shown in Eq. (8) and Taylor series expansion of E_{elec} with respect to $w_L/(H+R_{\text{ext}})$, the electrical spring constant is obtained as[44]

$$k_{\text{elec}} = -\left.\frac{\partial^2 E_{\text{elec}}}{\partial w_L^2}\right|_{w_L=0} = -\frac{208\pi\varepsilon_0(V_{\text{dc}}^2 + V_{\text{ac}}^2)L}{405(H+R_{\text{ext}})^2\xi^2}\left(1+\frac{2}{\xi}\right). \quad (15)$$

The tuned resonant frequency of the actuated nanotube cantilever is approximated by

$$\frac{\omega_{\text{tun}}}{\omega_n} \approx \sqrt{1 - 0.364\frac{(V_{\text{dc}}^2 + V_{\text{ac}}^2)}{V_{\text{SPI}}^2}\left(\frac{2}{\xi}+1\right)}. \quad (16)$$

From Eq. (16), we can clearly see that the tuned resonant frequency of the electrostatically actuated cantilever is lower than its natural frequency, i.e., $\omega_{\text{tun}} < \omega_n$, which is due to the negative spring constant effect of electrostatic interactions, as shown in Eq. (15). Equation (16) also reveals that both V_{dc} and V_{ac} have to satisfy the following condition in order to keep the system stable:

$$V_{\text{dc}}^2 + V_{\text{ac}}^2 < 2.747V_{\text{SPI}}^2\left(\frac{2}{\xi}+1\right)^{-1}. \quad (17)$$

Inserting Eq. (16) into Eq. (10), the S-S resonant oscillation of the nanotube cantilever is given by

$$\frac{S(D)}{\left(\frac{D}{H+R_{\text{ext}}}\right)^2} = \frac{0.549V_{\text{SPI}}^2}{QV_{\text{dc}}V_{\text{ac}}} \times \frac{L}{\xi^2}\sqrt{1 - 0.364\frac{(V_{\text{dc}}^2 + V_{\text{ac}}^2)}{V_{\text{SPI}}^2}\left(\frac{2}{\xi}+1\right)}. \quad (18)$$

The instability or RPI happens when

$$\frac{\partial(\Delta E_{\text{elec}} + \Delta E_{\text{damp}})}{\partial D} = 0. \quad (19)$$

From Eqs. (18) and (19), the RPI conditions are given by

$$\frac{S'(D_{\text{RPI}})}{\frac{2D_{\text{RPI}}}{(H+R_{\text{ext}})^2}} = \frac{0.549V_{\text{SPI}}^2 L}{QV_{\text{dc}}V_{\text{ac}}\xi^2} \times \sqrt{1 - 0.364\frac{(V_{\text{dc}}^2 + V_{\text{ac}}^2)}{V_{\text{SPI}}^2}\left(\frac{2}{\xi}+1\right)}. \quad (20)$$

Comparing Eq. (20) with Eq. (18), the RPI oscillation amplitude of the cantilever tip D_{RPI} can be obtained from

$$\frac{S'(D_{\text{RPI}})}{S(D_{\text{RPI}})} = \frac{2}{D_{\text{RPI}}}. \quad (21)$$

Equation (21) shows that D_{RPI} is independent of the driving voltages while dependent on the quantity H/R_{ext}. Figure 3 shows the normalized D_{RPI} as a function of H/R_{ext} ranging from 10 to 5000, as plotted based on the solution of Eq. (21). D_{RPI} increases monotonically from $0.832H$ to $0.900H$ with the increase in H/R_{ext} in the given range. It is noted that the RPI oscillation amplitude $D_{\text{RPI}} = 0.832H - 0.900H$ is substantially higher than its quasistatic pull-in limit $D_{\text{SPI}} = 0.66H$ (Ref. 42) and than the RPI limit $D_{\text{RPI}} = 0.54H$ of a double-sided driven MEMS gyroscope (a micro-plate resonator) reported by Seeger and Boser.[33] The large stable S-S oscillation range of the nanotube cantilever indicates a large stable operation range for the device, which is of importance to many of its applications.

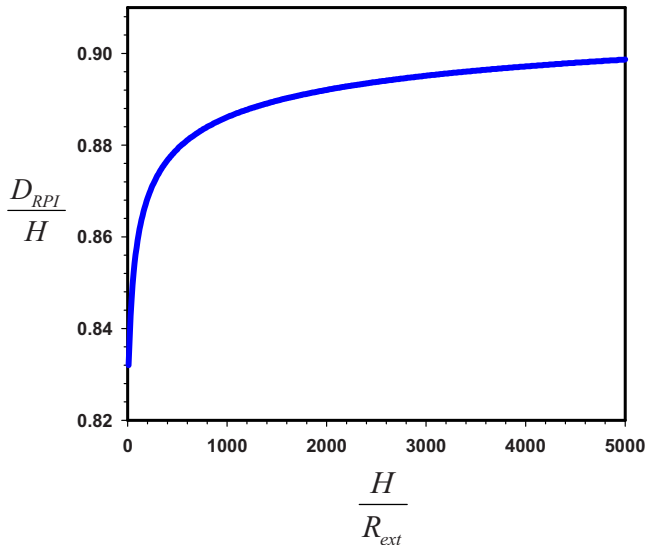

FIG. 3. (Color online) The dependence of the RPI oscillation amplitude of the cantilever tip on the quantity H/R_{ext}.

Both Eqs. (18) and (20) show that the S-S resonant oscillation and the RPI of this double-sided driven resonator are determined by both the dc and ac components of the driving signals. In the following section, we discuss the S-S resonant oscillation and the RPI of the resonator for two representative driving signals: (1) $V_{\text{dc}} = V_{\text{ac}}$ and (2) $V_{\text{dc}} \gg V_{\text{ac}}$.

III. CASE STUDY AND DISCUSSIONS

A. $V_{\text{dc}} = V_{\text{ac}}$

The driving signals applied on both electrodes become half-wave signals with a 180° difference between their phases, implying that the electrodes are becoming active alternatively. This type of driving signals has been utilized in the actuation of MEMS gyroscopes.[33] The S-S resonant oscillation of the nanotube cantilever is given by

$$\frac{S(D)}{\left(\frac{D}{H+R_{\text{ext}}}\right)^2} = \frac{0.549}{Q}\left(\frac{V_{\text{SPI}}}{V_{\text{dc}}}\right)^2 \times \frac{L}{\xi^2}\sqrt{1 - 0.728\left(\frac{V_{\text{dc}}}{V_{\text{SPI}}}\right)^2\left(\frac{2}{\xi}+1\right)}. \quad (22)$$

Equation (22) shows the correlation between the S-S resonant oscillation amplitude of the cantilever tip D and the driving voltage V_{dc} (and V_{ac}). We compare the analytical results based on Eq. (22) with the numerical results obtained

by solving Eq. (1) in predicting the S-S resonant oscillation and the RPI conditions.

We numerically solve Eq. (1) using the assumed-modes method,[45] which assumes a solution of Eq. (1) in the form $r(x,t)=\Sigma_{i=1}^{n}\eta_i(t)Y_i(x)$, in which $\eta_i(t)$ $(i=1,2,\ldots)$ are the modal coordinates and $Y_i(x)$ $(i=1,\ 2,\ldots)$ are the linear undamped mode shapes of the cantilever beam. $Y_i(x)$ is given by

$$Y_i(x)=T_i\left[\sin\beta_i x-\sinh\beta_i x-\frac{\sin\beta_i L+\sinh\beta_i L}{\cos\beta_i L+\cosh\beta_i L}(\cos\beta_i x-\cosh\beta_i x)\right],\quad i=1,\ 2,\ \ldots, \tag{23}$$

where β_i is the solution of the characteristic equation $\cos\beta_i L\cosh\beta_i L+1=0$ and T_i is a coefficient and can be obtained through the orthogonal properties of $Y_i(x)$, i.e., $\int_0^L\rho A Y_i^2(x)dx=1$. The modal coordinates $\eta_i(t)$ are given by[45]

$$\eta_i(t)=\frac{1}{\omega_i}\int_0^t N_i(t-\tau)\sin(\omega_i\tau)d\tau,\quad i=1,\ 2,\ \ldots, \tag{24}$$

in which

$$N_i(t)=\int_0^L Y_i(x)\left(q_{\text{elec}}(x,t)+q_{\text{vdW}}(x,t)-c\frac{dr(x,t)}{dt}\right)dx\quad(i=1,2,\ldots),$$

are the modal forces and ω_i is the ith natural frequency of the cantilever beam and is given by $\omega_i=\beta_i^2\sqrt{EI/\rho A}$. Therefore, $r(x,\ t)$ can be obtained as

$$r(x,t)=\sum_{i=1}^{n}\frac{Y_i(x)}{\omega_i}\int_0^t N_i(t-\tau)\sin(\omega_i\tau)d\tau,\quad r=1,2,\ldots. \tag{25}$$

We utilize five modes, i.e., $n=5$ in Eq. (25), in our numerical simulations.

We consider a nanotube-based resonator with the following parameters: $L=500$ nm, $R_{\text{int}}=1.4$ nm, and $R_{\text{out}}=3.075$ nm (six graphite layers assuming inner layer distance of 0.335 nm), $E=1$ TPa, $\rho=1350$ kg/m^3, $H=100$ nm, and $Q=1000$. Both electrodes are assumed to be 30-layer graphene sheets. The quasistatic pull-in voltage is calculated to be $V_{\text{SPI}}=4.06$ V. The natural frequency of the nanotube cantilever is $\omega_n=647\times10^6$ rad/s or $f_n=103$ MHz. In our numerical simulation, we determine the resonant frequency for each driving voltage using a frequency sweeping approach. When the nanotube cantilever oscillates at its tuned resonant frequency, its oscillation lags the driving voltage by 90° in phase. By monitoring the phase difference between the oscillation and the driving voltage, the tuned resonant frequency and the corresponding S-S oscillation amplitude can be determined from the phase and amplitude responses of the oscillating cantilever.

Figures 4(a) and 4(b) show the S-S oscillation amplitude and phase responses of the nanotube cantilever as a function of the driving frequency f for three driving voltages $V_{\text{dc}}=0.0183V_{\text{SPI}}$, $0.0193V_{\text{SPI}}$, and $0.0197V_{\text{SPI}}$, respectively. Because the tuned resonant frequency of the cantilever beam is $f_r<f_n$, in our simulation the driving frequency starts from f_n and decreases at a fixed interval, which is 800 Hz in our study. The y axis of Fig. 4(b), denoted as φ, represents the phase lag between the oscillation of the nanotube and the driving signal applied on electrode I. The tuned resonant frequency for each driving voltage corresponds to a 90° phase difference between the oscillation and the driving signal and is determined from the curves in Fig. 4(b). Subsequently, we obtain the oscillation amplitude of the nanotube cantilever oscillating at its tuned resonant frequency from Fig. 4(a). It is clear that the resonant frequency decreases with the increase in the driving voltages, while the resonant oscillation amplitude increases with the increase in the driving voltage. It is noted that the driving frequency corresponding to the peak (maximum) oscillation amplitude does not coincide with the tuned resonant frequency, which is due to a frequency shift caused by the damping in the system. However, when the Q factor is sufficiently large, the resonant oscillation amplitude is almost equal to the peak oscillation

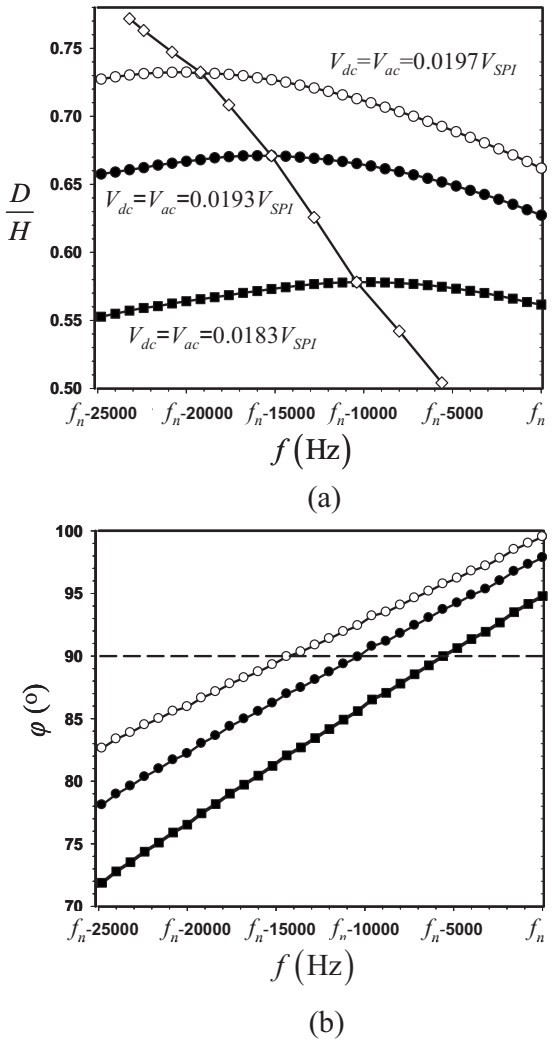

FIG. 4. The S-S oscillation (a) amplitude and (b) phase responses of the cantilever tip as a function of the driving frequency f for three given V_{dc} and V_{ac}. The diamond curve in (a) shows the dependence of the peak oscillation amplitude on the driving frequency.

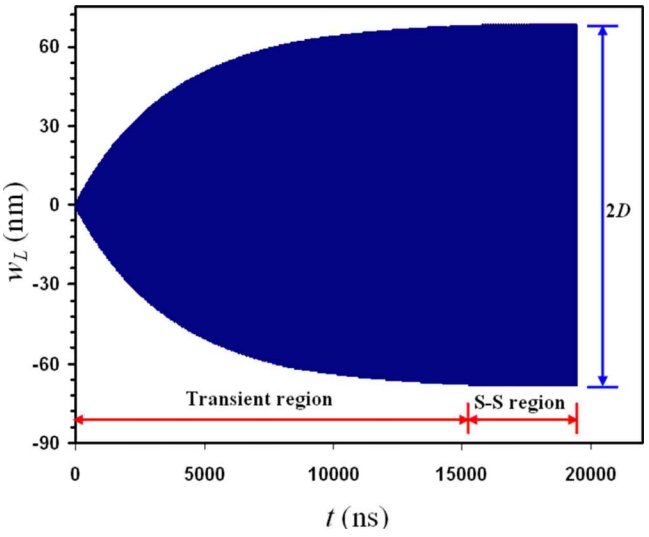

FIG. 5. (Color online) The motion of the cantilever tip as a function of time.

amplitude. The dependence of the peak oscillation amplitude on the driving frequency is shown in the diamond curve in Fig. 4(a). The oscillation of the cantilever tip obtained by our numerical simulations is exemplified in Fig. 5. The driving voltage is $V_{dc}=V_{ac}=0.0193V_{SPI}$ and the driving frequency is $f=f_n-10.4$ kHz, which is its tuned resonant frequency and corresponds to a S-S oscillation amplitude of about $0.67H$. It can be seen that the oscillation of the cantilever tip can be divided into two regions: the transient region and the S-S region. In the transient region, the oscillation amplitude increases monotonically with time, while in the S-S region, the oscillation amplitude stays in a constant mode. The S-S oscillation amplitude of the cantilever tip is half of the oscillation range of the cantilever tip in the S-S region.

Figure 6 shows a detailed view of a part of the S-S oscillation shown in Fig. 5. Figure 6 also illustrates the driving signal applied on electrode I. It can be seen that the oscillation of the cantilever tip in the S-S region is a

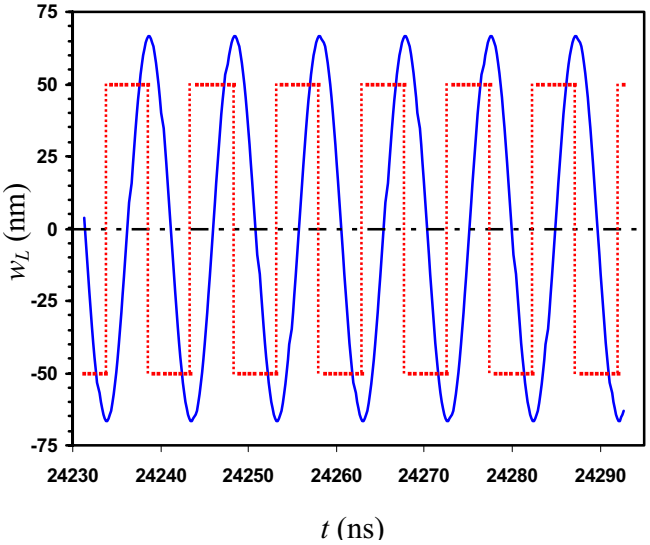

FIG. 6. (Color online) The motion of the cantilever tip in the S-S resonation (blue curve). The red dotted curve represents the square-wave driving signal applied on electrode I.

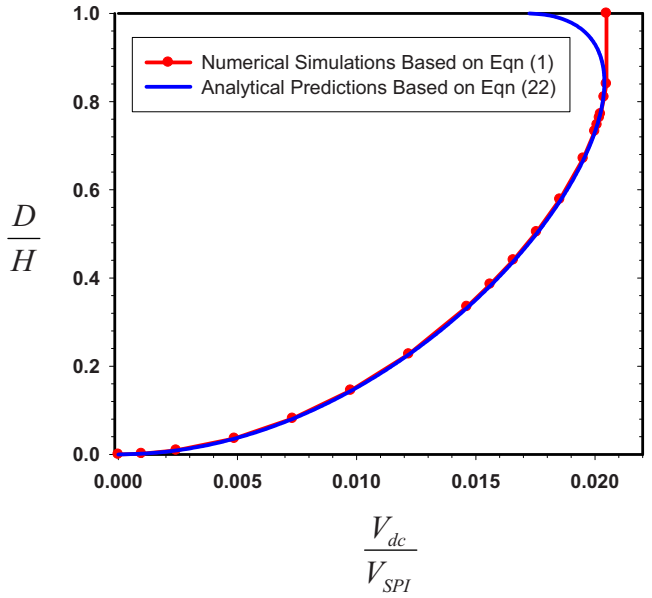

FIG. 7. (Color online) The S-S resonant characteristics, including RPI, of the double-sided driven resonator.

sinusoidal-like function with a phase lag of approximately 90° with respect to the driving signal, both of which are in good agreement with the aforementioned assumptions in deriving the closed-form analytical solutions.

Figure 7 illustrates the S-S electromechanical characteristics of the resonator obtained from the closed-form analytical solution given by Eq. (22). The analytical solution curve shows that the S-S resonation amplitude of the cantilever tip increases monotonically with the increase in the driving voltage until the driving voltage reaches its maximum. The maximum driving voltage is indicative of the occurrence of the resonant pull-in phenomenon. In the region close to the RPI, it is noticed from Fig. 7 that each driving voltage corresponds to two oscillation amplitudes. One is smaller than the RPI amplitude ($D_{RPI}=0.843H$), while the other is higher than the RPI amplitude. However, only the one smaller than the RPI amplitude is a stable solution, while the other is an unstable solution and can only be captured through the incorporation of a feedback control mechanism.[35,46] Figure 7 also shows a comparison between the analytical predictions and the numerical simulations, which are in good agreement in predicting both the S-S resonant oscillation and the RPI conditions. Both methods show that RPI voltage $V_{ac}^{RPI}=V_{dc}^{RPI}\approx 0.0204V_{SPI}$, which implies that the tuned resonant frequency is only slightly lower than its natural frequency based on Eq. (16). This observation is consistent with our numerical simulation results. On the other hand, it suggests that the resonant frequency tuning capability of the device for such driving signals is quite limited. The good agreement between the closed-form analytical solutions and the numerical simulations show that our closed-form analytical formulas can be used confidently in predicting the S-S resonant oscillation and the RPI conditions in such devices.

B. $V_{dc} \gg V_{ac}$

Under such driving voltages, the resonant frequency of the actuated nanotube cantilever ω_{tun} is mainly tuned by V_{dc} and is given by

$$\frac{\omega_{\text{tun}}}{\omega_n} \approx \sqrt{1 - 0.364\left(\frac{V_{\text{dc}}}{V_{\text{SPI}}}\right)^2\left(\frac{2}{\xi} + 1\right)}. \tag{26}$$

Equation (26) reveals that tuned resonant frequency ω_{tun} is inversely correlated with V_{dc}. The S-S resonant oscillation of the nanotube cantilever tip is given by

$$\frac{S(D)}{\left(\frac{D}{H + R_{\text{ext}}}\right)^2} = \frac{0.549 V_{\text{SPI}}^2 L}{Q V_{\text{dc}} V_{\text{ac}} \xi^2} \sqrt{1 - 0.364\left(\frac{V_{\text{dc}}}{V_{\text{SPI}}}\right)^2\left(\frac{2}{\xi} + 1\right)}. \tag{27}$$

Equation (27) shows that the stable S-S resonant oscillation amplitude of the cantilever tip D can be controlled by V_{ac}. Therefore, the processes of tuning the resonant frequency and controlling the stable S-S oscillation amplitude of the nanotube cantilever are decoupled and can be controlled separately by V_{dc} and V_{ac}, respectively. The maximum stable oscillation range of the cantilever tip, or twice of its RPI oscillation amplitude, is not affected by the electrostatic-force-induced frequency tuning. Such unique resonant frequency tuning capability is superior to the resonant frequency tuning in resonators with a single-sided excitation scheme.

For a cantilevered beam-based resonator with the single-sided excitation scheme, the constant force component in the driving electrostatic force induces a static deflection of the cantilever beam, reducing the gap between the cantilever and the electrode. Therefore, the maximum stable oscillation amplitude of the cantilever becomes smaller because the RPI phenomenon takes place at a smaller oscillation amplitude. Because the electrostatic-force-induced frequency tuning inevitably induces static deflection of the cantilevered beam, the maximum stable oscillation range of the cantilever is decreased by its static deflection. Such limitation on the stable oscillation range of the device becomes more severe when a large static deflection is induced as a result of the electrostatic-force-induced resonant frequency tuning, and therefore may negatively impact its applications. This limitation can be effectively avoided in the double-sided driven resonator as presented in this paper. The unique behavior in resonant frequency tuning associated with the double-sided excitation scheme makes the resonator attractive for many applications such as tunable sensors for ultratiny mass and forces and tunable electronics.

Using the aforementioned device parameters, we analyze the S-S resonant oscillation and the RPI conditions of the device for three different driving signals with their dc component V_{dc} fixed at $0.8V_{\text{SPI}}$, $1.0V_{\text{SPI}}$, and $1.2V_{\text{SPI}}$, respectively. Using Eq. (26), the corresponding tuned resonant frequencies are estimated to be $0.810\omega_n$, $0.680\omega_n$, and $0.475\omega_n$, respectively. Figure 8 shows the stable S-S resonant characteristics and RPI for all three driving voltages, which are plotted based on Eq. (27). The RPI limits of the ac component V_{ac} are found to be $4.21 \times 10^{-4} V_{\text{SPI}}$, $2.83 \times 10^{-4} V_{\text{SPI}}$, and $1.65 \times 10^{-4} V_{\text{SPI}}$, respectively. Our results show that the applied V_{ac} in the driving voltages for the stable S-S resonation of the device is much smaller than V_{dc}, implying that V_{ac} has little impact on the resonant frequency tuning. The pull-in

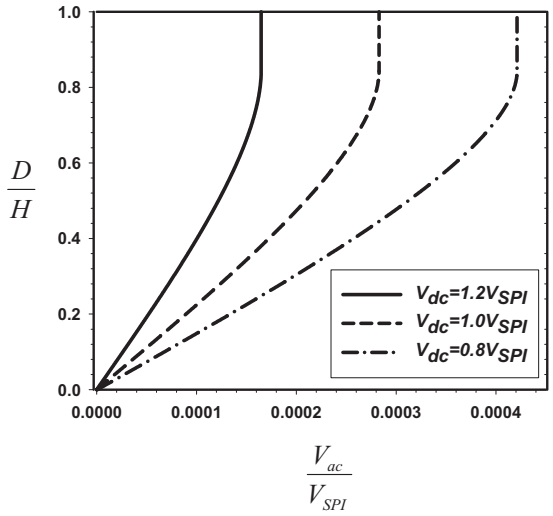

FIG. 8. The S-S resonant characteristics, including RPI, of the double-sided driven resonator for three tuned resonant frequencies by V_{dc}.

oscillation amplitude is $D_{\text{RPI}} = 0.843H$ for all three cases. All three curves shown in Fig. 8 display a linear relationship regarding the dependence of D on V_{ac} within a fairly large range, e.g., D from 0 to $0.6H$. Such linear correlation is useful to the control of the stable S-S oscillation amplitude of the resonator.

IV. THE LIMITATION OF THE CURRENT MODELS

There are several assumptions and simplifications in the theoretical model presented in this paper. The present model does not take in account the finite kinematics (large displacement) of the oscillating nanotube cantilever[39,42] or the concentration charges at the free end of the nanotube cantilever.[47] In addition, when the nanotube is on the order of a few nanometers in diameter, such as single-walled CNTs, the quantum effect becomes prominent and has to be taken into account in the calculation of the charge distribution on the surface of the nanotube because the density of states on the surface of the nanotube with a small diameter is limited and the electrical charges may penetrate inside the nanotube.[48] Though the aforementioned factors, if omitted, are expected to result in deviations in predicting the device's electromechanical dynamics, we believe that the results as presented in this paper regarding the overall S-S resonant oscillation and RPI behaviors of the resonator will not be substantially impacted.

V. CONCLUSION

In summary, in this paper, we investigate the electromechanical dynamics of a double-sided driven cantilevered nanotube-based electromechanical resonator. Closed-form analytical solutions capable of predicting the S-S resonant oscillation and the RPI conditions are derived using an energy-based method. They were then verified through a comparison with numerical simulations. Our results clearly reveal the device's electromechanical dynamics associated with the double-sided excitation scheme regarding the resonator's stable operation range and resonant frequency tuning.

The results reported in this paper will be useful to the optimal design of double-sided driven nanotube or nanowire base electromechanical resonators. The methodologies presented in this paper can be useful to study other novel nanoscale electromechanical systems.

ACKNOWLEDGMENTS

This work was supported by the State University of New York at Binghamton. The author thanks Dr. M. I. Younis and Mr. O. Loh for helpful discussions.

[1]C. T. C. Nguyen, L. P. B. Katehi, and G. M. Rebeiz, Proc. IEEE **86**, 1756 (1998).
[2]J. J. Yao, J. Micromech. Microeng. **10**, R9 (2000).
[3]G. T. A. Kovacs, *Micromachined Transducers Sourcebook* (McGraw-Hill, New York, 1998).
[4]B. Ilic, H. G. Craighead, S. Krylov, W. Senaratne, C. Ober, and P. Neuzil, J. Appl. Phys. **95**, 3694 (2004).
[5]V. Sazonova, Y. Yaish, H. Ustunel, D. Roundy, T. A. Arias, and P. L. McEuen, Nature (London) **431**, 284 (2004).
[6]S. J. Martin, M. A. Butler, J. J. Spates, M. A. Mitchell, and W. K. Schubert, J. Appl. Phys. **83**, 4589 (1998).
[7]B. Ilic, D. Czaplewski, H. G. Craighead, P. Neuzil, C. Campagnolo, and C. Batt, Appl. Phys. Lett. **77**, 450 (2000).
[8]J. Lee, J. Jang, D. Akin, C. A. Savran, and R. Bashir, Appl. Phys. Lett. **93**, 013901 (2008).
[9]S. Iijima, Nature (London) **354**, 56 (1991).
[10]D. Qian, G. J. Wagner, W. K. Liu, M. F. Yu, and R. S. Ruoff, Appl. Mech. Rev. **55**, 495 (2002).
[11]P. L. McEuen, M. S. Fuhrer, and H. K. Park, IEEE Trans. Nanotechnol. **1**, 78 (2002).
[12]J. W. Mintmire, B. I. Dunlap, and C. T. White, Phys. Rev. Lett. **68**, 631 (1992).
[13]T. W. Tombler, C. W. Zhou, L. Alexseyev, J. Kong, H. J. Dai, L. Liu, C. S. Jayanthi, M. J. Tang, and S. Y. Wu, Nature (London) **405**, 769 (2000).
[14]T. Kuzumaki and Y. Mitsuda, Appl. Phys. Lett. **85**, 1250 (2004).
[15]B. Liu, H. Jiang, H. T. Johnson, and Y. Huang, J. Mech. Phys. Solids **52**, 1 (2004).
[16]M. S. Dresselhaus, G. Dresselaus, and P. Avouris, *Carbon Nanotubes* (Springer, Berlin, 2001).
[17]J. Y. Huang, S. Chen, Z. Q. Wang, K. Kempa, Y. M. Wang, S. H. Jo, G. Chen, M. S. Dresselhaus, and Z. F. Ren, Nature (London) **439**, 281 (2006).
[18]P. Poncharal, Z. L. Wang, D. Ugarte, and W. A. de Heer, Science **283**, 1513 (1999).
[19]H. B. Peng, C. W. Chang, S. Aloni, T. D. Yuzvinsky, and A. Zettl, Phys. Rev. Lett. **97**, 087203 (2006).
[20]Z. Tang, Y. Xu, G. Li, and N. R. Aluru, J. Appl. Phys. **97**, 114304 (2005).
[21]H. W. C. Postma, I. Kozinsky, A. Husain, and M. L. Roukes, Appl. Phys. Lett. **86**, 223105 (2005).
[22]M. Dequesnes, Z. Tang, and N. R. Aluru, J. Eng. Mater. Technol. **126**, 230 (2004).
[23]W. G. Conley, A. Raman, C. M. Krousgrill, and S. Mohammadi, Nano Lett. **8**, 1590 (2008).
[24]D. Garcia-Sanchez, A. S. Paulo, M. J. Esplandiu, F. Perez-Murano, L. Forro, A. Aguasca, and A. Bachtold, Phys. Rev. Lett. **99**, 085501 (2007).
[25]A. Husain, J. Hone, H. W. C. Postma, X. M. H. Huang, T. Drake, M. Barbic, A. Scherer, and M. L. Roukes, Appl. Phys. Lett. **83**, 1240 (2003).
[26]S. S. Verbridge, H. G. Craighead, and J. M. Parpia, Appl. Phys. Lett. **92**, 013112 (2008).
[27]S. S. Verbridge, R. I. H. G. Craighead, and J. M. Parpia, Appl. Phys. Lett. **93**, 013101 (2008).
[28]M. W. Li, R. B. Bhiladvala, T. J. Morrow, J. A. Sioss, K. K. Lew, J. M. Redwing, C. D. Keating, and T. S. Mayer, Nat. Nanotechnol. **3**, 88 (2008).
[29]X. L. Feng, R. R. He, P. D. Yang, and M. L. Roukes, Nano Lett. **7**, 1953 (2007).
[30]X. L. Feng, C. J. White, A. Hajimiri, and M. L. Roukes, Nat. Nanotechnol. **3**, 342 (2008).
[31]I. Kozinsky, H. W. C. Postma, I. Bargatin, and M. L. Roukes, Appl. Phys. Lett. **88**, 253101 (2006).
[32]K. Jensen, C. Girit, W. Mickelson, and A. Zettl, Phys. Rev. Lett. **96**, 215503 (2006).
[33]J. I. Seeger and B. E. Boser, *Parallel-Plate Driven Oscillations and Resonant Pull-In* (Solid-State Sensor, Actuator and Microsystems Workshop, Hilton Head Island, SC), June 2–6, 2002, pp. 313–316.
[34]R. N. Miles and R. R. Hoy, Audiol. Neuro-Otol. **11**, 86 (2006).
[35]M. Bao, *Analysis and Design Principles of MEMS Devices* (Elsevier, Amsterdam, 2005).
[36]J. Yu and S. Lee, H01L 27/115 (2006.01) ed. (Korea, 2007).
[37]A. H. Nayfeh, M. I. Younis, and E. M. Abdel-Rahman, Nonlinear Dyn. **48**, 153 (2007).
[38]M. Dequesnes, S. V. Rotkin, and N. R. Aluru, Nanotechnology **13**, 120 (2002).
[39]C. H. Ke, H. D. Espinosa, and N. Pugno, J. Appl. Mech. **72**, 726 (2005).
[40]W. Hayt and J. Buck, *Engineering Electromagnetics*, 6th ed. (McGraw-Hill, New York, 2001).
[41]J. E. Lennard-Jones, Proc. R. Soc. London, Ser. A **129**, 598 (1930).
[42]C. H. Ke, N. Pugno, B. Peng, and H. D. Espinosa, J. Mech. Phys. Solids **53**, 1314 (2005).
[43]N. Pugno, C. H. Ke, and H. D. Espinosa, J. Appl. Mech. **72**, 445 (2005).
[44]C. H. Ke and M. Zheng (unpublished).
[45]L. Meirovitch, *Fundaments of Vibrations* (Thomas Casson, New York, 2001).
[46]C. H. Ke and H. D. Espinosa, Appl. Phys. Lett. **85**, 681 (2004).
[47]C. H. Ke and H. D. Espinosa, J. Appl. Mech. **72**, 721 (2005).
[48]S. V. Rotkin, V. Shrivastava, K. A. Bulashevich, and N. R. Aluru, Int. J. Nanosci. **1**, 337 (2002).